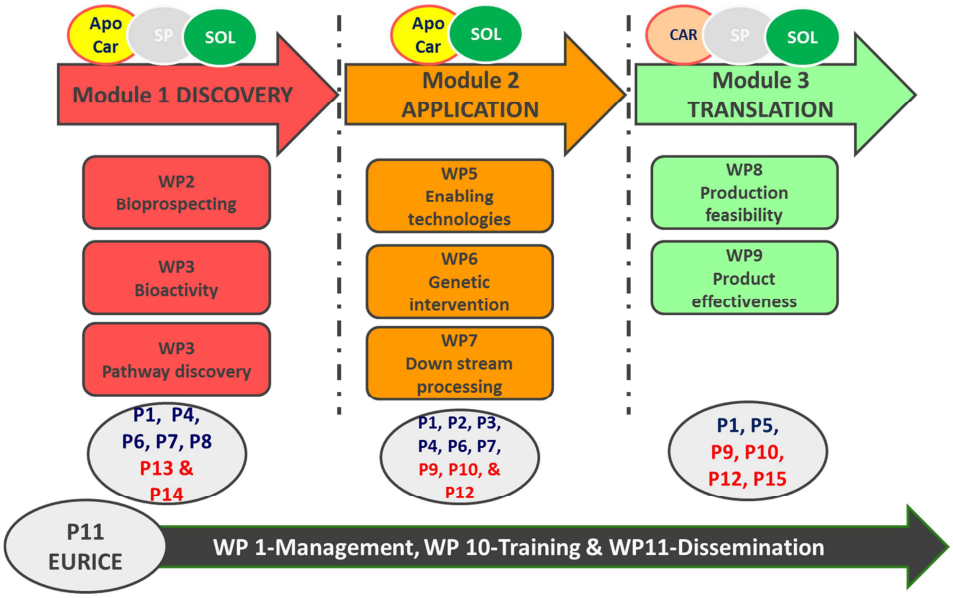

Figure 1. Showing the generic DISCO pipeline: Entry points of the target molecules and how fundamental science and innovation can add value to the supply chain are illustrated via the positioning of the WP activities.

(A) Literature survey on Iridaceae bioactive molecules

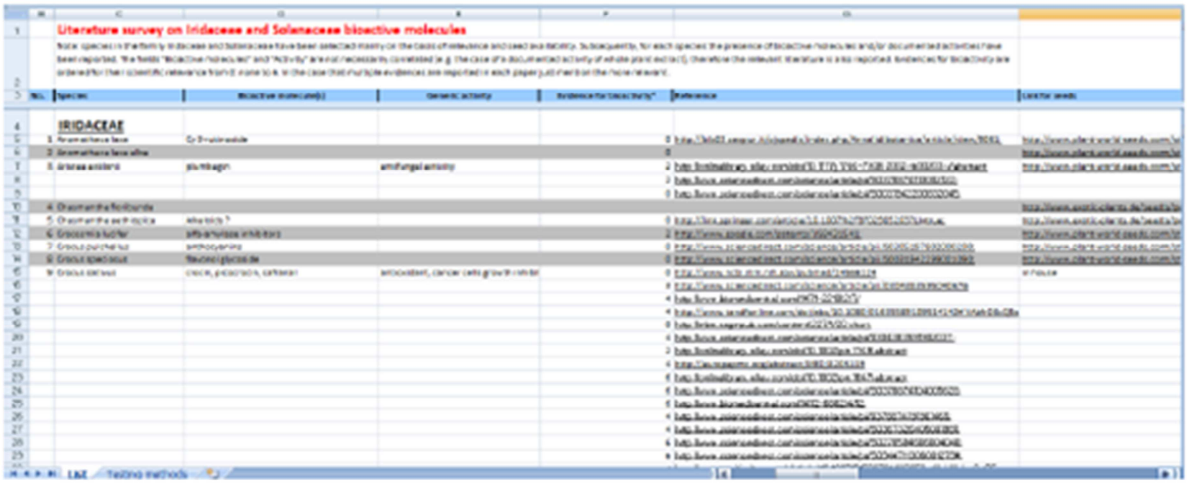

(B) Literature survey on Solanaceae bioactive molecules

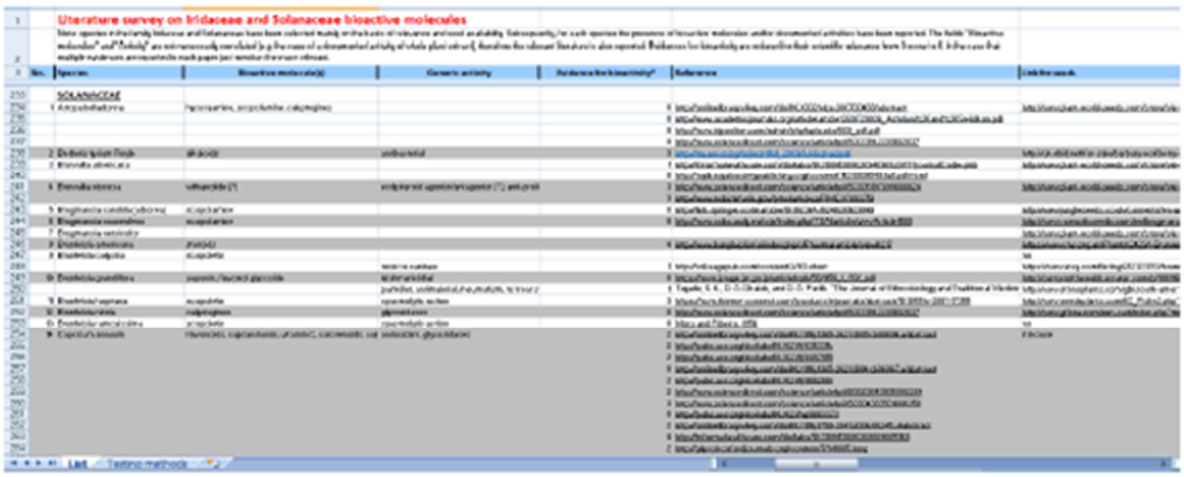

Figure 2. Demonstrating how the database was formatted using the first 9 *Iridaceae* species (out of 124 species found) **(A)** and first 14 *Solanaceae* species (out of 117) **(B)**. The data base lists the species, the associated bioactivity

found, active molecule if known, references reporting this information and source of seeds if known. There is also a numerical scale to indicate how reliable the evidence for the bioactivity was (0=not available, 1=anecdotal, 2 =cell free, 3=cell based, 4=animal testing, 5=epidemiology, 6=human tested). The full database contains a total of 241 species with 714 supporting references.

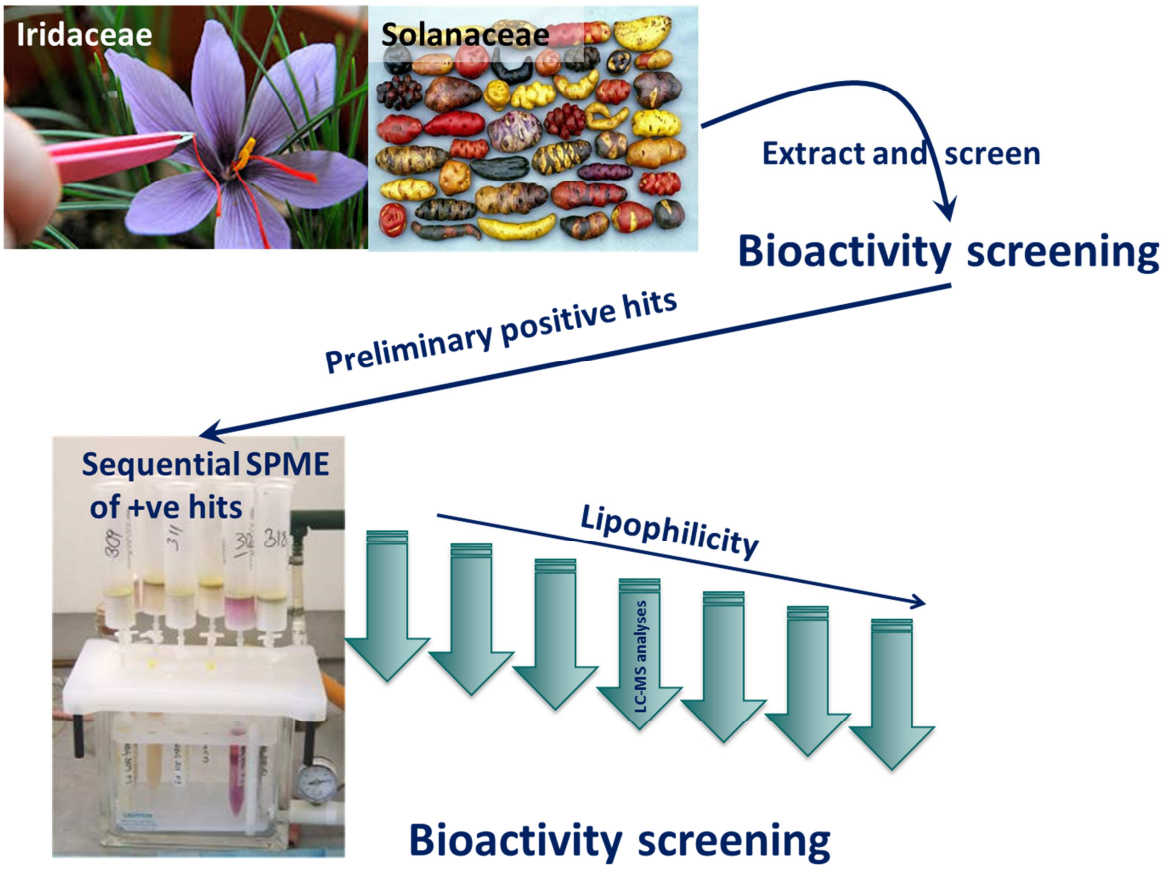

Figure 3. A schematic of germplasm screening and target optimisation against state of the art.

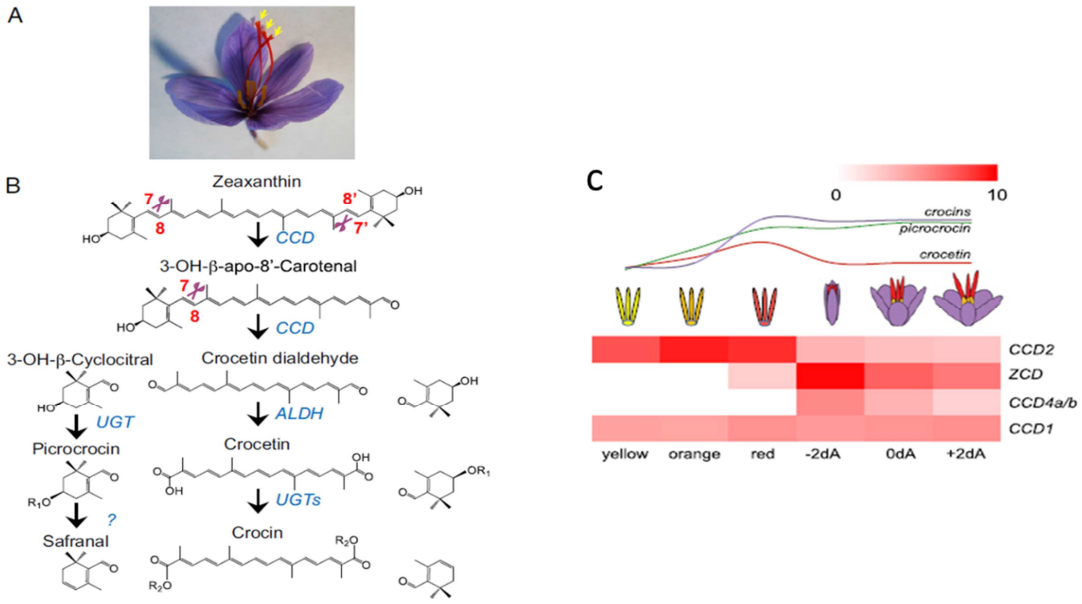

Figure 4. (A) The saffron apocarotenoid pathway. *Crocus sativus* flower at anthesis. The yellow arrowheads point at the three stigmas. **(B)** Proposed saffron apocarotenoid biosynthesis pathway. Zeaxanthin is cleaved at the 7,8 and 7',8'

positions by a CCD activity. The C20 cleavage product, crocetin dialdehyde, is converted to crocetin by an aldehyde dehydrogenase, and then to crocins by at least two UDPG-glucosyltransferases. The C10 product, 3-OH-β-cyclocitral, is converted to picrocrocin by an UDPG-glucosyltransferase, and then to safranal. **(C)** The expression patterns of the putative dioxygenases deduced from RNA-Seq datasets.

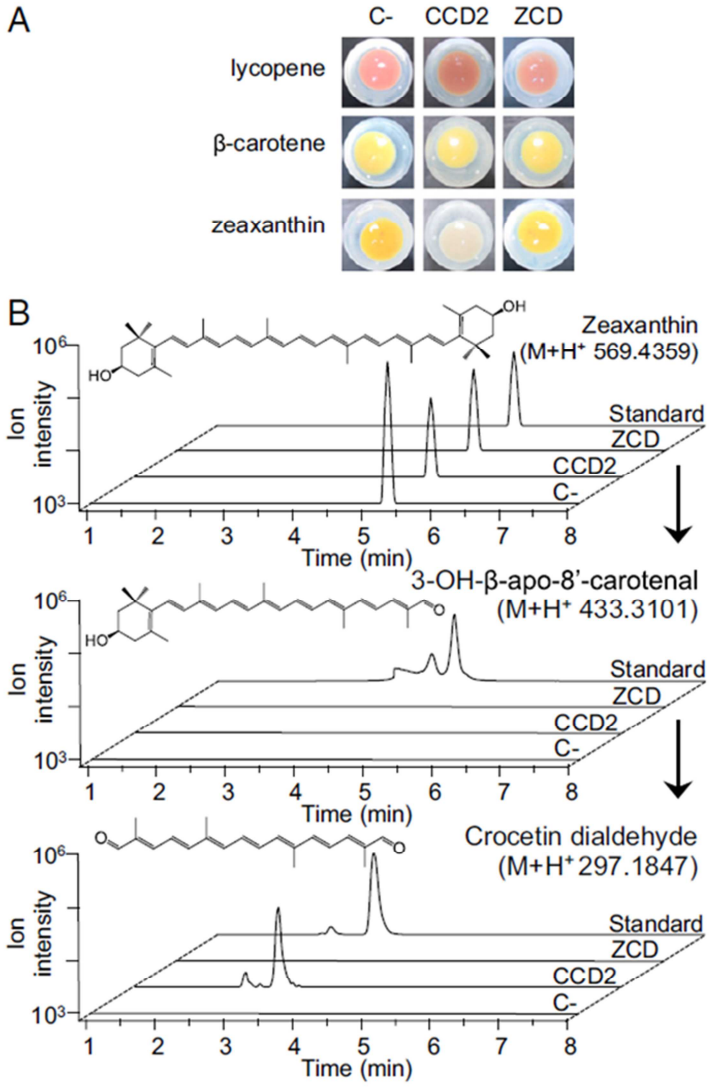

Figure 5. The figure illustrates CCD2 expressed in *E. coli* cleaves zeaxanthin to yield crocetin dialdehyde. **(A)** *E. coli* cells accumulating lycopene, β-carotene, or zeaxanthin were transformed with the empty pThio vector, C-, or the same vector expressing CCD2 or ZCD, induced for 16 h at 20 °C with arabinose and pelleted. Note the discoloration of zeaxanthin in CsCCD2-expressing cells. **(B)** LC-HRMS analysis of zeaxanthin cleavage products. Zeaxanthin-accumulating *E. coli* cells expressing CsCCD2 were induced for 16 h at 20 °C with arabinose, extracted with acetone, and the extracts were run on a LC-HRMS system alongside authentic standards. The accurate masses of zeaxanthin, 3-OH- β-apo-8'-carotenal, and crocetin dialdehyde were extracted. Only crocetin dialdehyde is detectable and has an accurate mass and a chromatographic mobility identical to that of the authentic standard.

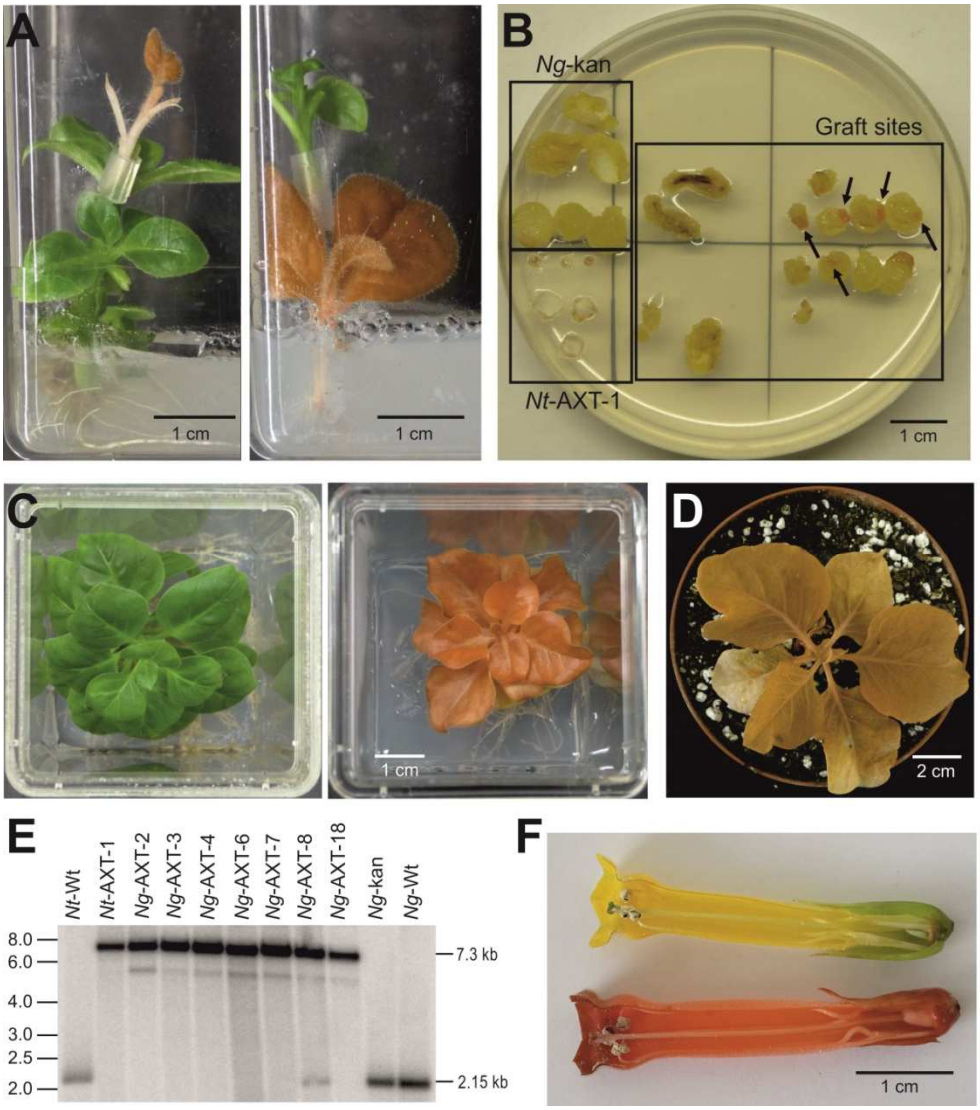

Figure 6. Transfer of the synthetic astaxanthin operon from *N. tabacum* to *N. glauca* by horizontal genome transfer. (**A**) Reciprocal grafting of the transplastomic astaxanthin-producing *N. tabacum* line (*Nt*-AXT-1) with a kanamycin-resistant *N. glauca* line (*Ng*-kan). (**B**) Detection of horizontal genome transfer on regeneration medium containing kanamycin and spectinomycin. The control explants (stem sections and leaf pieces) from the two graft partners are in the two left frames, the excised graft sites are in the right frame. Growing orange calli (indicated by arrows) indicate horizontal genome transfer events. Note that the *Nt*-AXT-1 control explants lost their orange color due to their sensitivity to kanamycin, a potent inhibitor of chloroplast translation. (**C**) Growth of regenerated transplastomic astaxanthin-synthesizing *N. glauca* plants (right) in comparison to a plant of the *Ng*-kan line used for grafting (left). (**D**) An astaxanthin-synthesizing *N. glauca* plant after transfer to the greenhouse. (**E**) Confirmation of horizontal genome transfer by RFLP analysis. RFLP analysis of 7 independent horizontal genome transfer lines of *N. glauca* (*Ng*-AXT lines) detects the same 7.3 kb fragment that is present in the transplastomic *N. tabacum* line used for grafting (*Nt*-AXT-1). Note that line *Ng*-AXT-8 is heteroplasmic and still contains copies of the resident *N. glauca* plastid genome, as evidenced by presence of the hybridization signal at 2.15 kb. (**F**) Flower phenotypes of an *N. glauca* wild-type plant (upper flower) and an *Ng*-AXT line (lower flower). Expression of the astaxanthin operon converts the yellow pigment of wild-type flowers (mainly lutein) into red astaxanthin (figure from Lu et al., 2017).

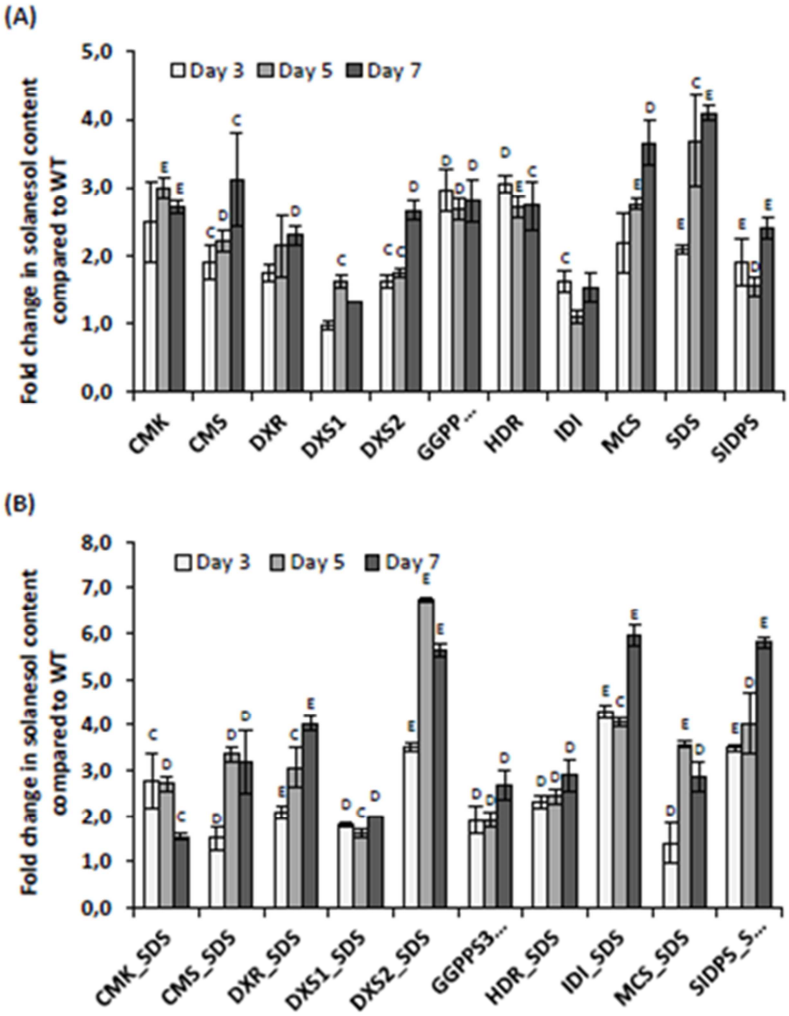

Figure 7. Comparison of the relative fold changes in leaf solanesol content relative to the mock inoculated WT *N. benthamiana* plants, in plants **(A)** transiently expressing single MEP pathway genes and **(B)** co-expression of MEP pathway gene and SDS. Values shown are presented at 3 time points and are the mean of three biological replicates. Statistical analysis was performed using Student's t-test and the significances are indicated (c) P <0.05, (d) P <0.01, (d) P <0.001.

In addition to pathway engineering, regulators of plastid parameters/core metabolism (*DE-ETIOLATED* (*DET*-1) and *GOLDEN LIKE* (*GLK*-1)) showed increased solanesol content. This could be due to improved supply of precursors from primary to secondary metabolism, CO_2 fixation and sequestration properties. In tomato natural variation (alleles) were determined as high accumulator of (up to 4 fold) levels of solanesol in vegetative tissues. Natural variation in potato was also carried out to identify potentially alleles having a positive positive effect on solanesol content.

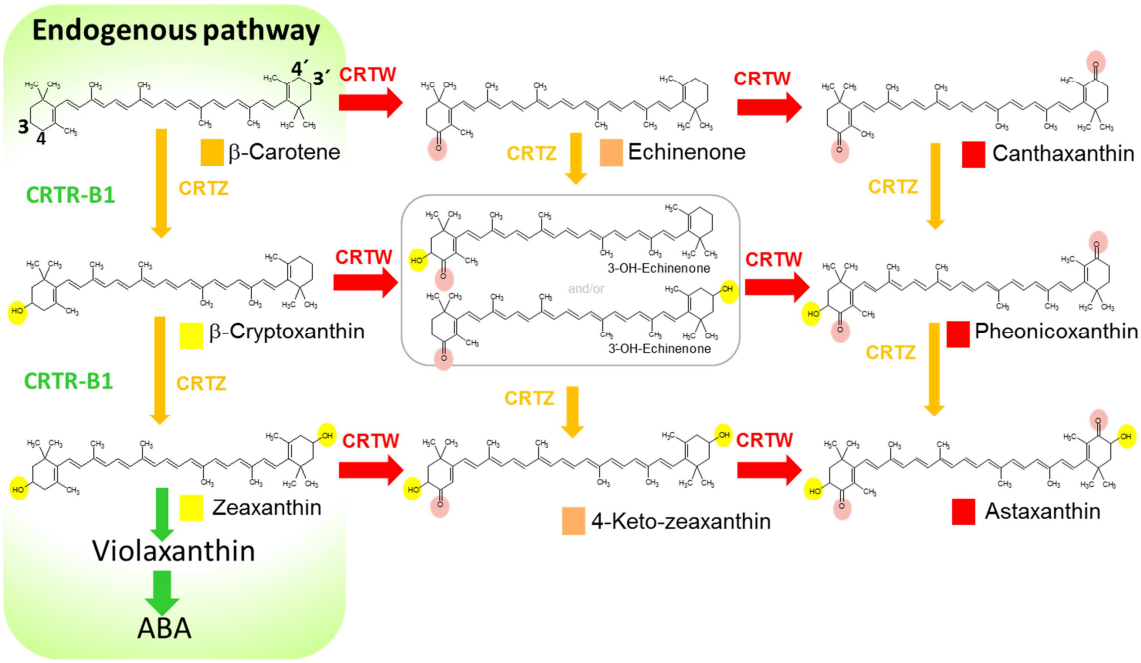

Figure 8. Representative scheme of the ketocarotenoid pathway introduced in plant. Enzyme names are as follow: CRTR-B1, plant carotene beta-hydroxylase 1; CRTW, bacterial carotene ketolase and CRTZ, bacterial carotene hydroxylase. The purple and blue shadings depict the position of the newly added functional group (hydroxyl or ketone, respectively).

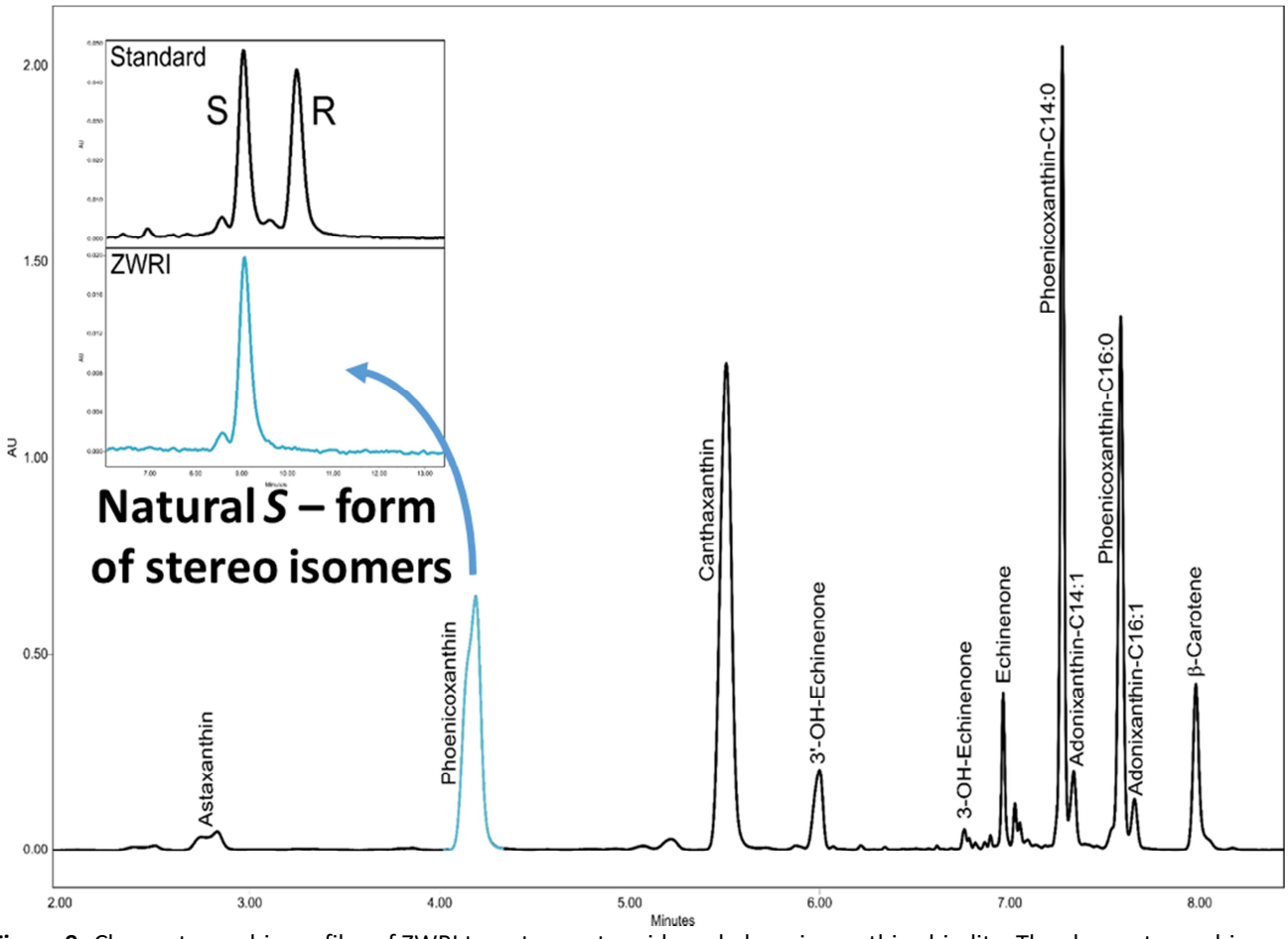

Figure 9. Chromatographic profiles of ZWRI tomato carotenoids and phoenicoxanthin chirality. The chromatographic carotenoids profile was obtained by UPLC and recorded at 470 nm. The insert shows that the chiral carbon of the ZWRI phoenicoxanthin has an *S* configuration.

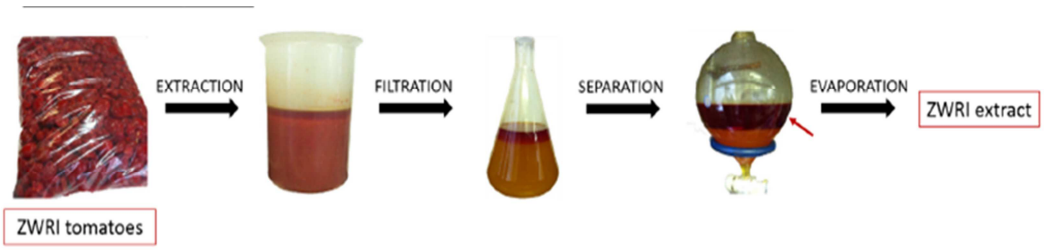

Figure 10. Illustrating the traditional extraction of carotenoids from the tomato based material.

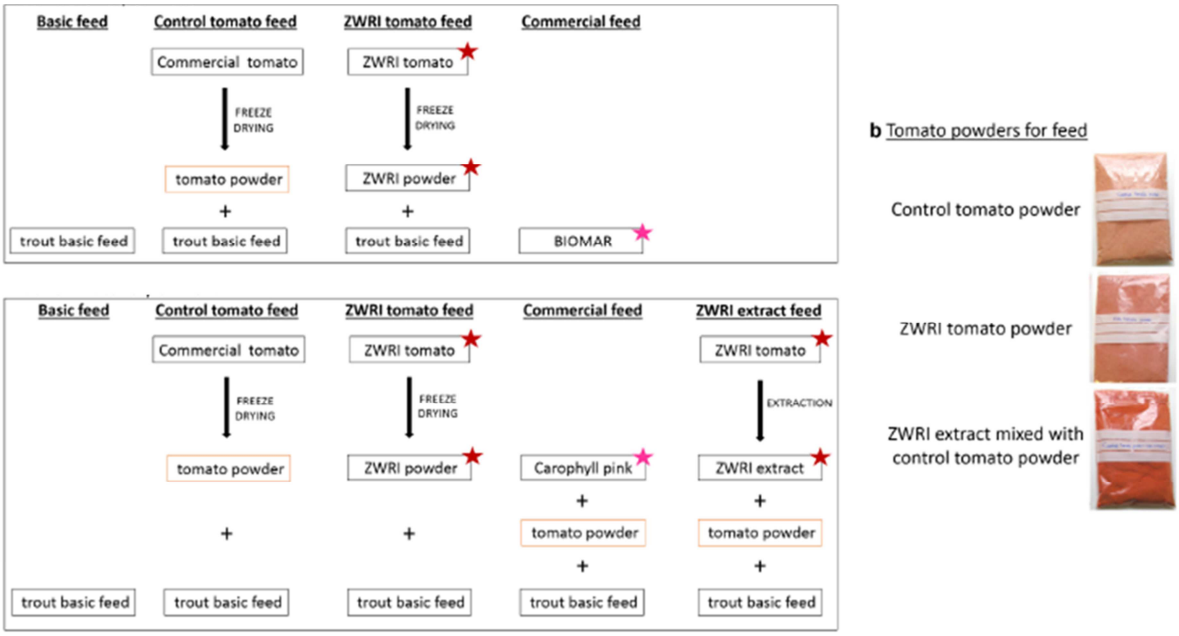

Figure 11. Workflow illustrating the minimal bioprocessing of the tomato derived material into effective aquaculture feed.

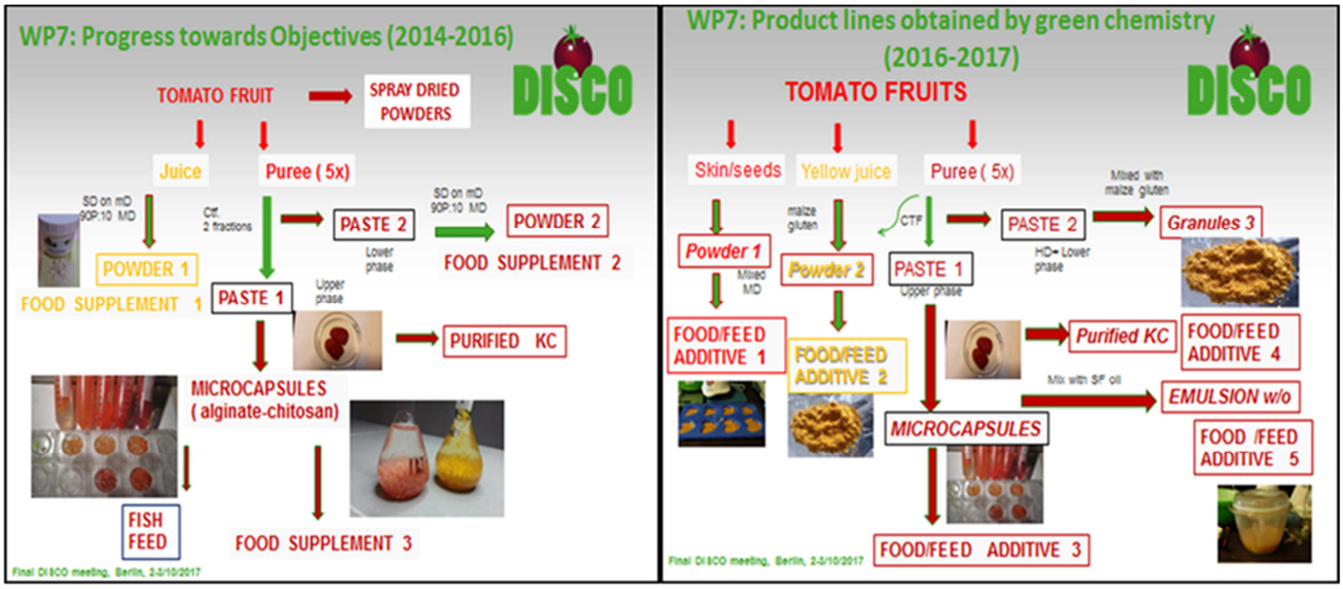

Figure 12. Initial down-stream processing and formulations followed by prototype products created with green chemistry

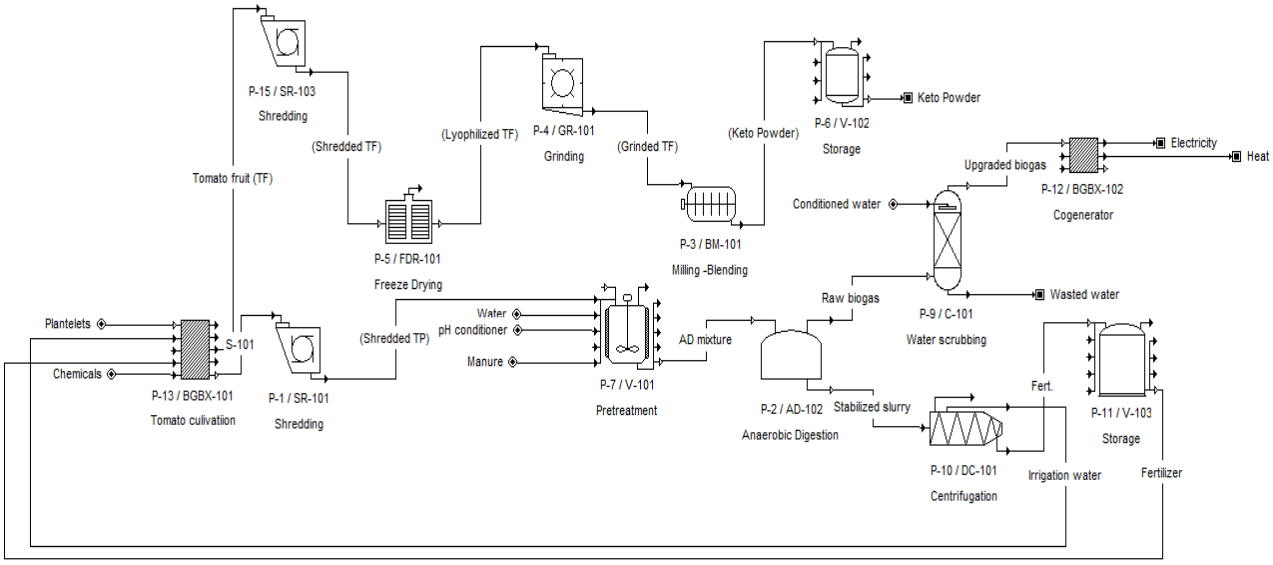

Figure 13. Simplified process flowsheet proposed for biogas production using tomato plant residues.

Figure 14. Polytunnel cultivation of DISCO prototypes; minimal resources input was used.

Table 1. Carotenoid content in ZWRI tomato line and azygous controls grown in greenhouse or polytunnel conditions. Carotenoid levels are represented as µg/g dry weight and in bold figures as percentages. Three representative fruits of *N* plants were used. The fruits were respectively pooled and three determinations were made. The mean data are shown as ± SD. Nq signifies that a compound has been detected but it is under the level of quantification. Polytunnel condition are defined by a polytunnel structure, without extra heating and lighting. Computed p-values for the comparison of ZWRI tomatoes grown in the greenhouse and the polytunnel are tabulated.

	Greenhouse								Polytunnel					
Carotenoid (µg/g DW)	ZWØRIØ	%	ZWØRI	%	ZWRIØ	%	ZWRI	%	ZWRI early season	%	ZWRI late season	%	Standard tomato	%
Phytoene	667 ±245	**12**	97 ±13	**6**	68 ±22	**2**	79 ±20	**2**	77 ±7	**3**	42 ±5	**2**	36 ±5	**2**
Phytofluene	644 ±173	**11**	111 ±10	**7**	463 ±161	**14**	73 ±3	**2**	84 ±3	**3**	65 ±3	**3**	296 ±93	**13**
Neurosporene	nq	nq	100 ±2	**6**	nq	nq	nq	nq	nq	nq	nq	nq	nq	nq
cis-Lycopene	91 ±27	**2**	nq	nq	nq	nq	nq	nq	nq	nq	nq	nq	73 ±11	**3**
Lycopene	3859 ±625	**68**	61 ±18	**4**	2543 ±411	**77**	nq	nq	nq	nq	nq	nq	1476 ±339	**67**
γ-Carotene	72 ±7	**1**	72 ±4	**4**	nq	nq	nq	nq	nq	nq	nq	nq	78 ±1	**4**
β-Cryptoxanthin	nq	nq	nq	nq	48 ±13	**1**	nq	nq	nq	nq	nq	nq	nq	nq
β-Carotene	205 ±86	**4**	1112 ±122	**66**	41 ±3	**1**	266 ±54	**8**	390 ±34	**14**	11 ±2	**8**	120 ±8	**5**
δ-Carotene	nq	nq	nq	nq	51 ±6	**2**	nq	nq	nq	nq	nq	nq	86 ±1	**4**
Lutein	155 ±11	**3**	143 ±7	**8**	nq	nq	nq	nq	nq	nq	nq	nq	151 ±27	**7**
Echinenone	nq	nq	nq	nq	nq	nq	76 ±10	**2**	96 ±9	**3**	54 ±7	**3**	nq	nq
3-OH-Echinenone	nq	nq	nq	nq	nq	nq	17 ±2	**1**	19 ±3	**1**	12 ±1	**1**	nq	nq
3'-OH-Echinenone	nq	nq	nq	nq	nq	nq	125 ±19	**4**	105 ±46	**4**	98 ±14	**5**	nq	nq
Canthaxanthin	nq	nq	nq	nq	8 ±8	**0**	899 ±151	**28**	873 ±62	**31**	634 ±144	**32**	nq	nq
Phoenicoxanthin	nq	nq	nq	nq	15 ±6	**0**	594 ±142	**18**	478 ±27	**17**	335 ±54	**17**	nq	nq
Astaxanthin	nq	nq	nq	nq	47 ±9	**1**	83 ±15	**3**	80 ±4	**3**	47 ±4	**2**	nq	nq
Phoenicoxanthin-C14:0	nq	nq	nq	nq	nq		553 ±79	**17**	300 ±20	**11**	183 ±38	**9**		
Phoenicoxanthin-C16:0	nq	nq	nq	nq	nq		298 ±54	**9**	174 ±21	**6**	209 ±76	**11**		
Adonixanthin-C14:1	nq	nq	nq	nq	nq	nq	130 ±27	**4**	106 ±14	**4**	72 ±27	**4**	nq	nq
Adonixanthin-C16:1	nq	nq	nq	nq	nq	nq	71 ±18	**2**	63 ±16	**3**	57 ±7	**3**	nq	nq
Total ketocarotenoids	0	**0**	0	**0**	74 ±30	**2**	2845 ±353	**87**	2294 ±163	**81**	1701 ±252	**86**	0	**0**
Total	5693 ±805	nq	1697 ±105	nq	3287 ±341	nq	3263 ±398	nq	2846 ±185	nq	1971 ±275	nq	2217 ±572	nq
N	3		3		5		4		4		4		3	

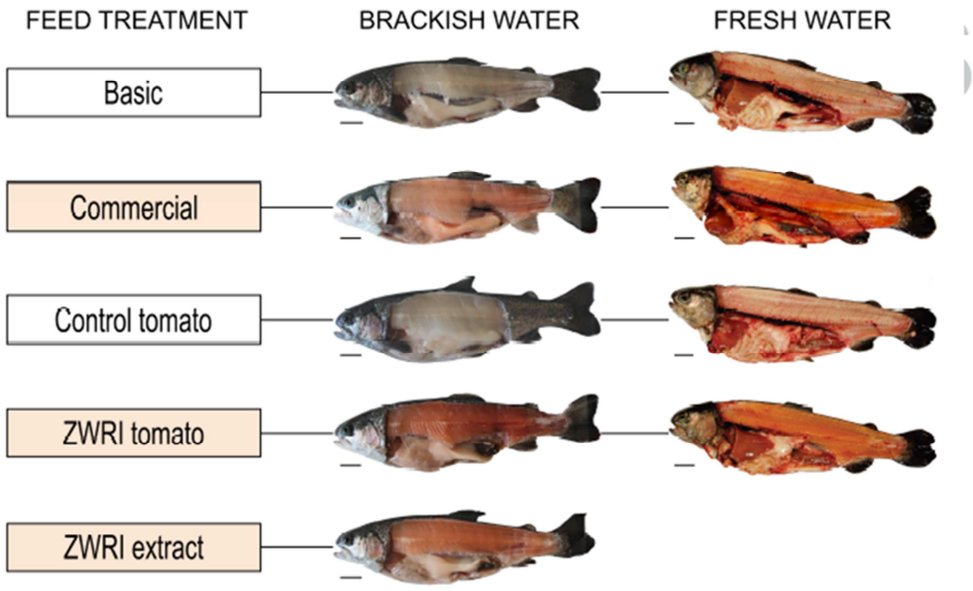

Figure 15. ZWRI tomatoes color trout fillets. Photographs of the trout fed with the basic, commercial, control tomato, ZWRI tomato and ZWRI extract feeds, taken at the end of the fresh and brackish water trials (50 and 80 days, respectively).

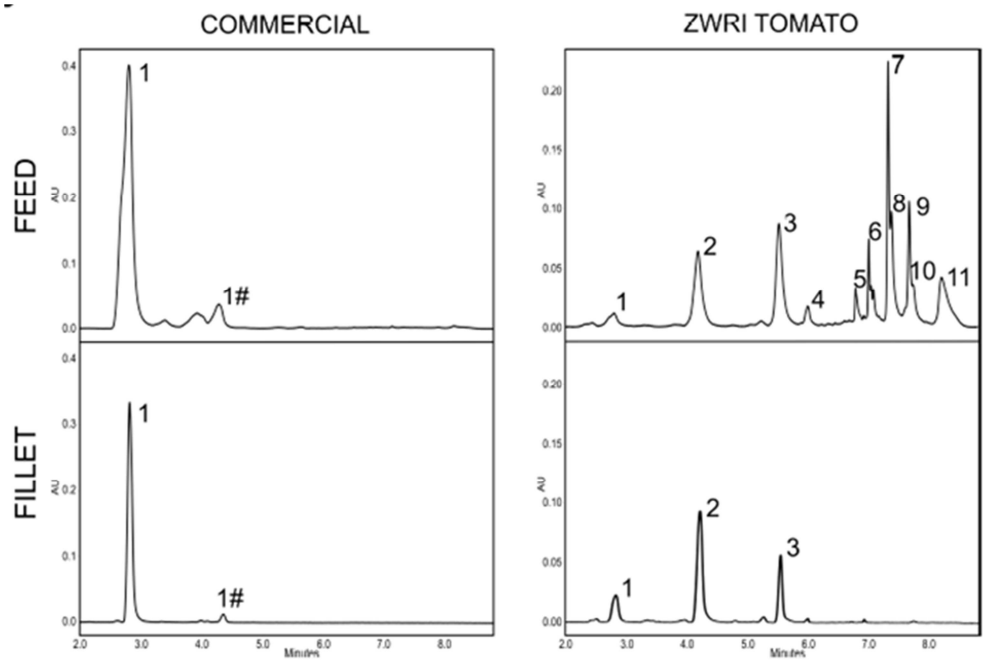

Figure 16. Chromatographic profiles of carotenoids in the feed and fillet corresponding to the commercial and ZWRI tomato treatments. 1, astaxanthin; 1#, unknown ketocarotenoid-1; 2, phoenicoxanthin; 3, canthaxanthin; 4, 3′-OH-echinenone; 5, 3-OH-echinenone; 6, echinenone; 7, phoenicoxanthin-C14:0; 8, adonixanthin-C14:1; 9, phoenicoxanthin-C16:0; 10, adonixanthin-C16:1; 11, β-carotene.

Fig. 17 A

PNAS

Efficient metabolic pathway engineering in transgenic tobacco and tomato plastids with synthetic multigene operons

Yinghong Lu, Habib Rijzaani[1], Daniel Karcher, Stephanie Ruf, and Ralph Bock[2]

Max-Planck-Institut für Molekulare Pflanzenphysiologie, D-14476 Potsdam-Golm, Germany

AUTHOR SUMMARY

Fig. 17 B

PNAS

Novel carotenoid cleavage dioxygenase catalyzes the first dedicated step in saffron crocin biosynthesis

Sarah Frusciante[a,b], Gianfranco Diretto[a], Mark Bruno[c], Paola Ferrante[a], Marco Pietrella[a], Alfonso Prado-Cabrero[d], Angela Rubio-Moraga[e], Peter Beyer[c], Lourdes Gomez-Gomez[e], Salim Al-Babili[c,d], and Giovanni Giuliano[a,1]

[a]Italian National Agency for New Technologies, Energy, and Sustainable Development, Casaccia Research Centre, 00123 Rome, Italy; [b]Sapienza, University of Rome, 00185 Rome, Italy; [c]Faculty of Biology, University of Freiburg, D-79104 Freiburg, Germany; [d]Center for Desert Agriculture, Division of Biological and Environmental Science and Engineering, King Abdullah University of Science and Technology, Thuwal 23955-6900, Saudi Arabia; and [e]Instituto Botánico, Facultad de Farmacia, Universidad de Castilla–La Mancha, 02071 Albacete, Spain

Fig. 17 C

PNAS

Engineering of tomato for the sustainable production of ketocarotenoids and its evaluation in aquaculture feed

Marilise Nogueira[a], Eugenia M. A. Enfissi[a], Maria E. Martínez Valenzuela[b], Guillaume N. Menard[c], Richard L. Driller[b], Peter J. Eastmond[c], Wolfgang Schuch[b], Gerhard Sandmann[d], and Paul D. Fraser[a,1]

[a]School of Biological Sciences, Royal Holloway University of London, Egham, Surrey TW20 0EX, United Kingdom; [b]Fraunhofer Chile Research, Las Condes, Santiago 7550296, Chile; [c]Plant Sciences, Rothamsted Research, Harpenden AL5 2JQ, United Kingdom; and [d]Biosynthesis Group, Molecular Biosciences, Goethe University Frankfurt, 60323 Frankfurt, Germany

Figure 17. Examples of publications in high impact peer reviewed journals.

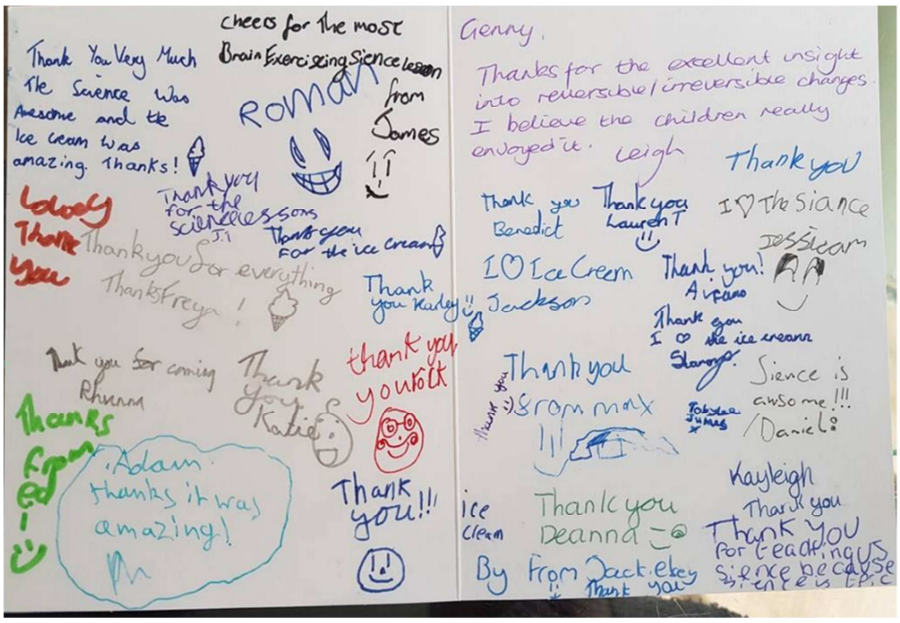

Figure 18. Thank you card for the practical activities provided for primary school children.

Figure 19. An example recent scientific advances incorporated into the scientific curriculum in Europe.

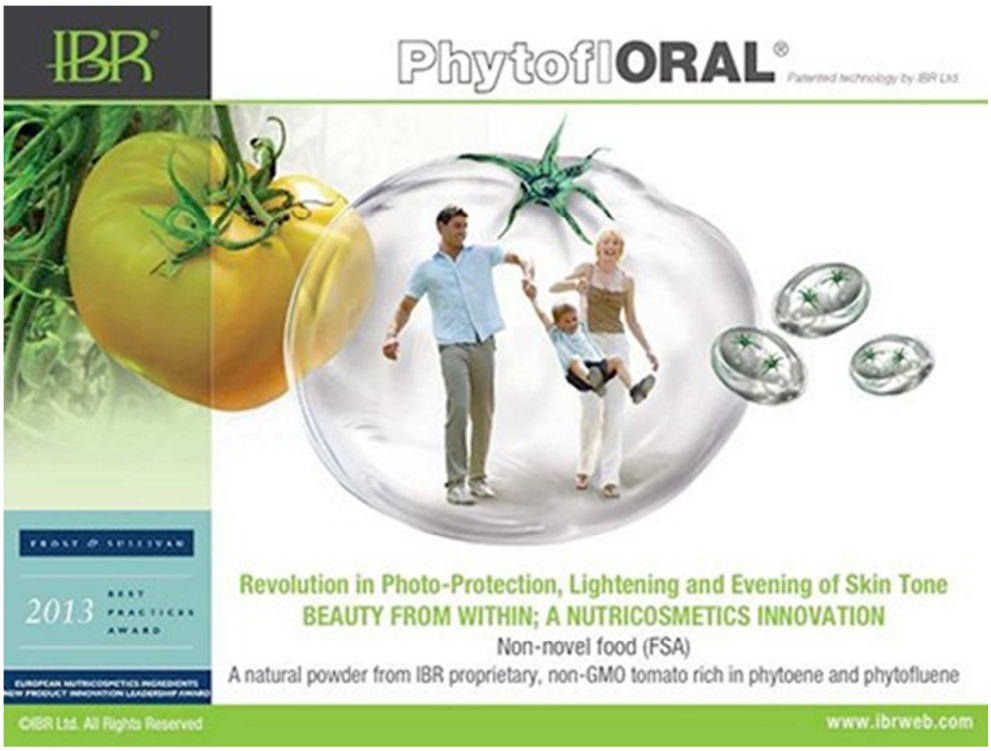

Figure 20. DISCO derived innovation product development by P12-IBR and P3-HUJI.

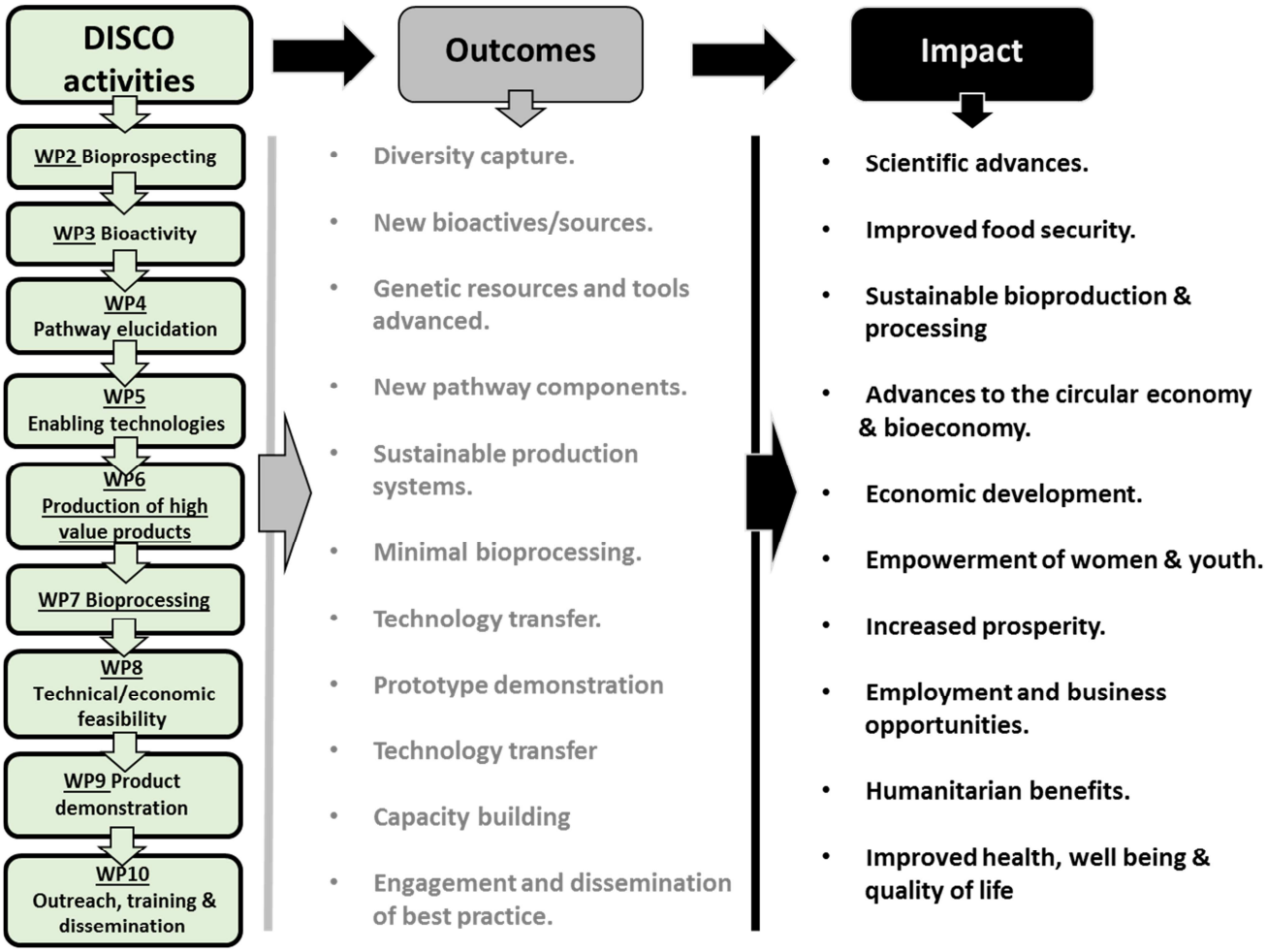

Figure 21: DISCO interconnectivity of programme activities, outcomes and delivery of impact.